Optically Excited CSACs with Integrated Nanoresonators

John Kitching and Leo Hollberg
Time and Frequency Division, NIST
325 Broadway, Boulder, CO 80305
kitching@boulder.nist.gov

Semi-Annual Report for the Period: 10/03-2/04

Research carried out with support from DARPA's program on Chip-Scale Atomic Clocks (CSAC)

Key Accomplishments (9/03-1/04):

1. Developed integrated optics and heating assemblies for CSAC physics package
2. Fabricated a preliminary vertically-integrated CSAC physics package
    a. Fractional frequency instability: 3×10^{-10} at one second
    b. Size: 9.5 mm^3
    c. Power dissipation: 71 mW, not including power to heat laser
    d. Magnetic shielding and longitudinal magnetic field applied externally
3. Carried out thermal analysis of vertically integrated structure to evaluate possibility for low-power operation
    a. Identified gold wire-bonds as major heat-loss channel
    b. Anticipate power required to heat the cell could be reduced to 12 mW by advanced thermal engineering.

Objectives for next six months (2/04-8/04):

1. To carry out a full evaluation of the CSAC performance including
    a. Limits to long term stability such as pressure shift, AC Stark shift and cell-temperature issues
    b. Optimization of short-term stability and evaluation of sources of noise
2. To run the CSAC as a CPT magnetometer and evaluate the performance limits
3. To design and build an advanced physics package with the following upgrades
    a. Integrated temperature sensor for cell temperature stabilization
    b. Advanced thermal isolation spacer for low-power operation
    c. Vacuum packaging and integrated magnetic shielding
    d. Advanced heater design to reduce magnetic fields
4. Begin collaborations with other groups to integrate NIST physics package with small, low-power local oscillators and control electronics
5. Begin collecting data on direct coupling of atoms to mechanically resonant microstructures by exciting Zeeman transitions between atomic spin states.

Introduction and Background

The goals of the NIST/CU chip-scale atomic clock (CSAC) program are to develop a compact physics package consistent with the DARPA program requirements and to investigate basic physics and core technologies related to CSAC. The NIST physics package under development is based on a micro-machined atomic confinement cell and all-optical excitation of the atoms using a vertical-cavity surface-emitting laser (VCSEL). The ultimate design goals are a total physics package volume of 3 mm^3, a power dissipation of 20 mW and a fractional frequency instability of 10^{-10} at one second, integrating down to 1×10^{-11} at one hour. The basic physics package design is shown in Figure 1.

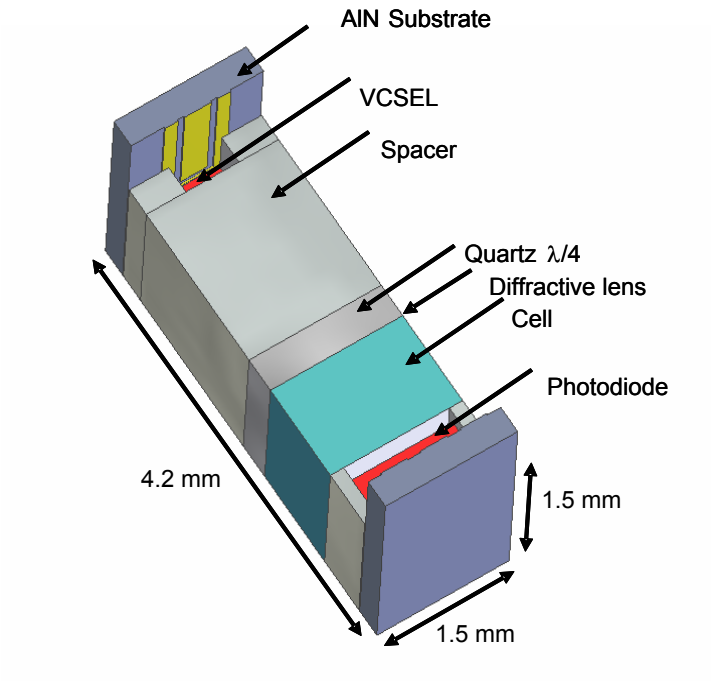

Figure 1. Schematic of the proposed CSAC physics package. The three main components of the physics package, the laser, the cell and the detector, will be contained within a volume of 3 mm^3.

The atomic excitation scheme for our design is shown schematically in Figure 2. In 2001, NIST constructed a compact prototype frequency reference based on coherent population trapping (CPT) resonances. A photograph of this prototype is shown in Figure 3. NIST's program seeks essentially to further miniaturize this type of frequency reference by incorporating MEMS technology into the methods for fabricating components. The key tasks NIST identified as critical to the success of this miniaturization program were: cell miniaturization using MEMS, wall coatings and atom-surface interactions to preserve the atomic coherence, micro-optical components and assembly and the direct coupling of atoms to micro-resonator structures. We discuss each of these aspects in turn in the subsequent parts of this document.

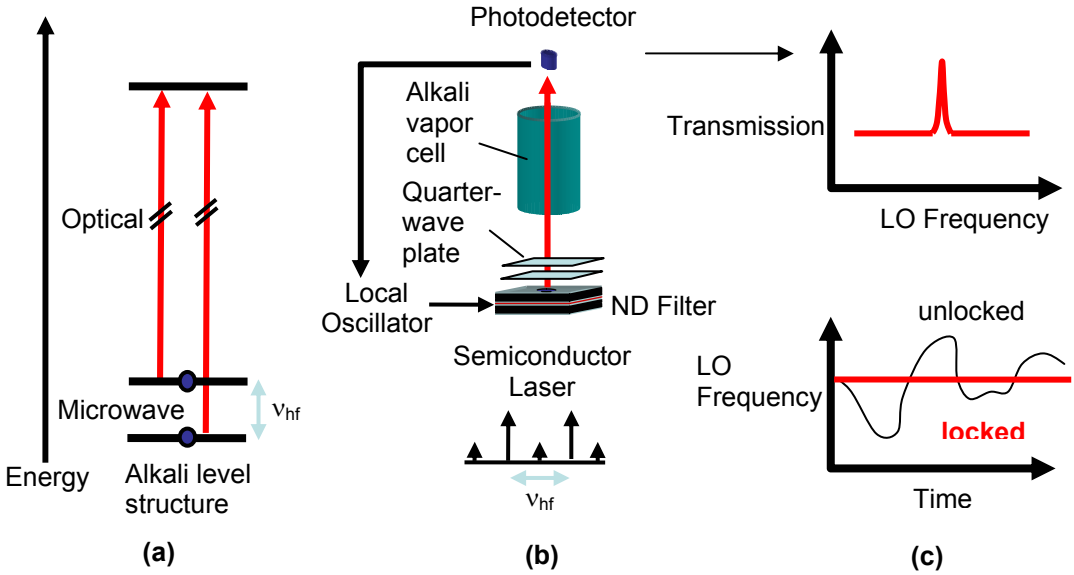

Figure 2 Schematic for modulation and excitation of atoms. (a) The atomic energy levels and laser tunings required to excite the CPT resonance. (b) The injection current of a diode laser is modulated at one-half the atomic hyperfine splitting. The two first-order optical sidebands excite a CPT resonance in the atomic cell, which is detected as shown in (c) by monitoring the power transmitted through the cell. When the modulation frequency coincides with the atomic resonance frequency, the change in power that occurs can be used to lock the local oscillation (which provides the modulation) to the atomic resonance.

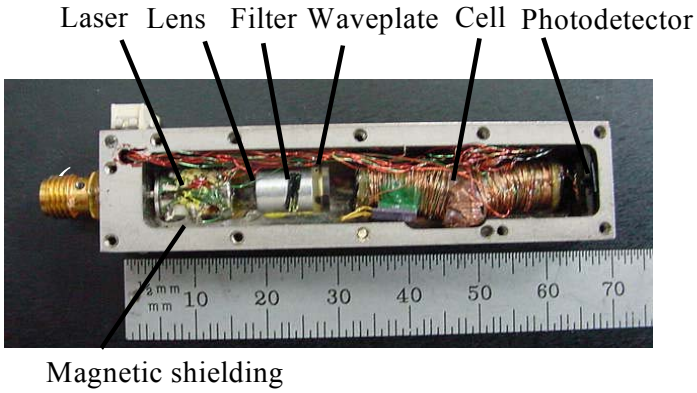

Figure 3 The NIST compact atomic clock based on coherent population trapping, built in 2001.

Description of Progress

Task 1: Cell Miniaturization

The task of cell miniaturization has, for the most part, been successfully accomplished. NIST now has several methods of fabricating compact alkali-atom vapor cells appropriate for use in atomic frequency references, as outlined in the previous report (Sept. 2003). The method we currently use to fabricate our cells is based on anodic bonding of Si and glass wafers. Holes are etched or drilled in the wafers and glass is bonded onto one side. Cs metal is introduced into the cell using the reaction $BaN_6 + CsCl \rightarrow BaCl + 3N_2 + Cs$. A second window is then bonded to the top of the cell, sealing the Cs, along with an appropriate buffer-gas pressure inside. A photograph of a diced cell made at NIST is shown in Figure 4.

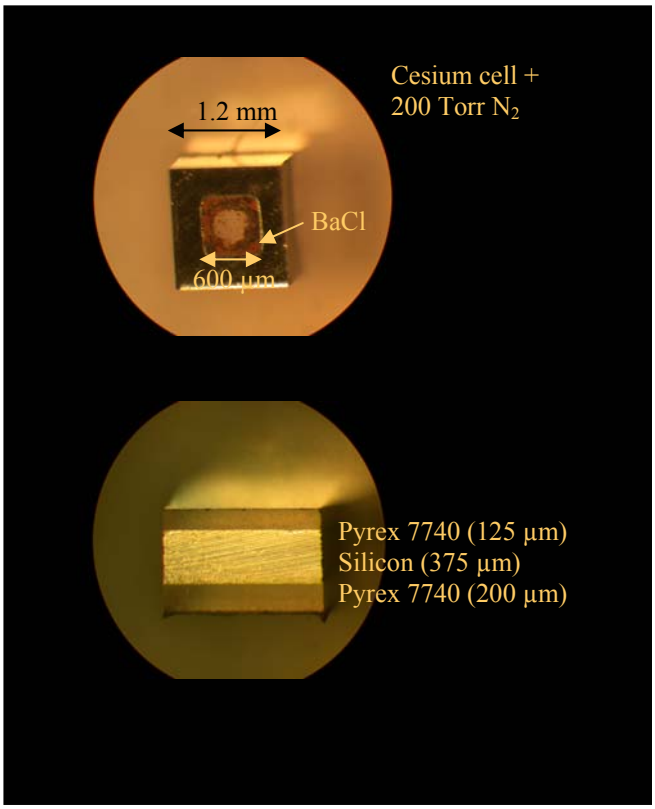

Figure 4 Diced, compact vapor cells fabricated using anodic bonding is Si and glass.

We are beginning to explore two other methods of filling the cells. The first is based on a thermal beam of Cs atoms, which is directed towards the cell preforms in a high-vacuum system. The Cs atoms are deposited through a shadow mask as a thin film on the interior surface of the cell array. The mask is then removed and a second glass layer is bonded to the surface to seal the atoms inside the cell. A second method involves the diffusion of alkali atoms into the cell from a thermal vapor through a porous membrane.

Task 3b: Direct Coupling of Atoms to Microresonators

This component of the project consists of an experiment to generate magnetic coupling between a microresonator and a sample of atoms. The microresonator is a magnetic-tipped, MEMS-fabricated cantilever, and the atom sample is made up of laser-cooled Rb atoms. Our first attempt to demonstrate direct coupling is to create an oscillating magnetic field with the oscillating cantilever, which will drive transitions between different magnetic states in the atom sample. We also plan to conduct the "inverse" experiment, in which we will modulate the polarization of the atom sample, thereby changing the response of the oscillating cantilever. These experiments provide a unique opportunity to study the interaction between a classical micromechanical resonator and a group of atoms obeying the laws of quantum mechanics. Possible practical applications of the direct coupling experiment are in the chip-scale atomic clock and miniature magnetometers.

We have made significant progress in the first phase of the direct coupling experiment. The preliminary design and construction of the laser-cooling apparatus are completed. Starting from a room temperature atomic vapor, we use a magneto-optical trap (MOT) to capture up to N=3x10^8 atoms and cool them to a temperature T~200 μK (see Fig. 1 below). These laser-cooled atoms have an average lifetime in the trap of 1.5 sec, limited by collisions with hot background gas atoms. The lifetime of the atoms is long enough to allow us to drop them into a separate interaction chamber where the atoms then approach the oscillating cantilever. Since the atoms must fall a distance of 20 cm to reach the cantilever, the fall time is only 0.2 s, or 1/8 of the atom lifetime. Thus we expect to lose only a small fraction (1-exp[-1/8])=0.12 of the atoms during their travel time.

We have also implemented an optical molasses after the MOT to further cool the atoms down below 5 μK. At such a low temperature, the average atomic velocity is only 2 cm/s, so the cloud of cold atoms will only expand its volume by a factor of 8 during the fall time. This means that the density of atoms in the interaction region will be big enough to see a large atomic resonance signal due to the microresonator's oscillating magnetic field.

Finally, construction of the microresonator, a double-torsional cantilever shaped like a two-segmented paddle, is proceeding. We have designed and created masks for the etching and fabrication process, and we plan to make a production run in the near future.

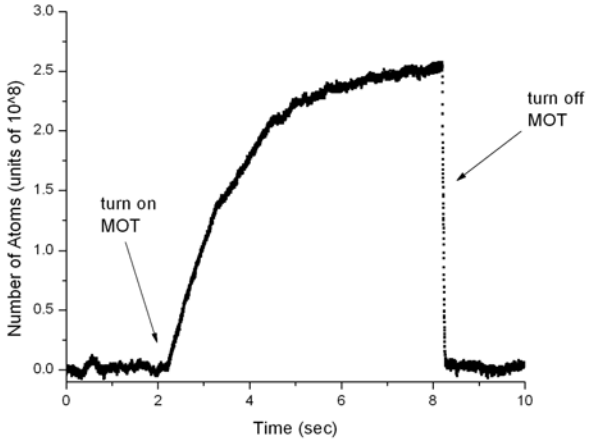

Figure 5 Loading atoms into the MOT. The line shows the number of atoms held in the MOT as a function of time. The arrows indicate when the trap is turned on and off. The time constant for the exponential loading process is 1.5 sec, which is the same as the average lifetime of an atom in the MOT.

Task 4: Optical Subsystem

The optical subsystem provides the light required to excite the CPT resonance and conditions the light before it enters the cell. The light is generated by a vertical-cavity surface-emitting laser (VCSEL) die emitting at 852 nm and mounted on an gold-coated alumina baseplate. The DC laser current and RF modulation are injected through a coplanar waveguide patterned in the gold, to which the laser top contact is wire-bonded. The laser is tuned to the optical transition in Cs by adjusting both the temperature and DC laser injection current. For the CSAC described here, the laser bias current was 1.3 mA and the laser baseplate was heated to 46 ºC. The RF power at 4.6 GHz injected into the laser was 70 μW and was sufficient to produce optimal modulation of the laser optical field.

A schematic of the light conditioning assembly is shown in Figure 6a. It is composed of five basic layers. The lowest layer was a spacer unit designed both to keep the collimating lens the appropriate distance from the laser facet and to thermally isolate the cell assembly from the baseplate. This thermal isolation was needed to ensure that the power required to keep the cell at its operating temperature was low. The spacer unit consisted of two glass walls, 1.5 mm long and 175 μm wide. The thermal conductance of this spacer unit was about 1.5 mW/K and therefore was expected to dissipate roughly 51 mW to maintain a temperature difference of 35 ºC between the cell and the baseplate. The additional thermal isolation provided by the glass layers above the spacer, reduced this power dissipation to about 30 mW. Above the lower spacer was a neutral-density (ND) filter that provided a first stage of optical attenuation before the light entered the cell. This ND filter was a piece of optically thick glass, 0.5 mm thick. A micro-refractive lens was mounted on top of the ND filter. Lenses such as this are commercially available in arrays and are fabricated by inkjet deposition of optical epoxy onto a glass substrate. The lens used here had a diameter of 0.9 mm and a focal length of about 0.7 mm, as measured from its flat surface. Around the lens, a second spacer unit was placed to create

a flat surface above the lens onto which additional components could be mounted. This spacer was a piece of 0.5 mm-thick Si with a hole etched in the center by deep reactive-ion etching (DRIE). On top of the Si spacer a piece of quartz was mounted. The quartz was 70 μm thick and served well as a low-order quarter-wave-plate at 850 nm. A second ND filter was mounted on top of the waveplate to attenuate the light even further. At the output of the micro-optics assembly, therefore, was a beam of light ~ 250 μm in diameter at its half-power point, with circular polarization and a power of 12 μW. Photographs of the optics subassembly are shown in Figure 6b and Figure 6c.

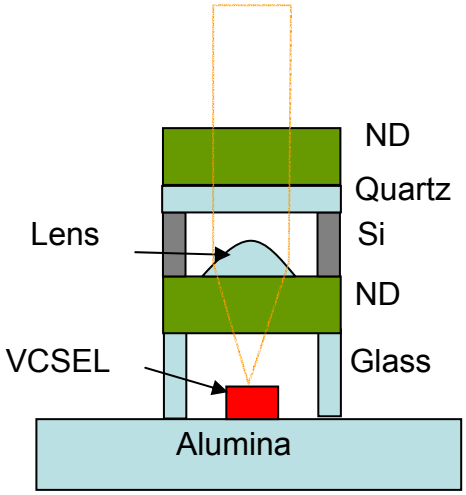

(a)

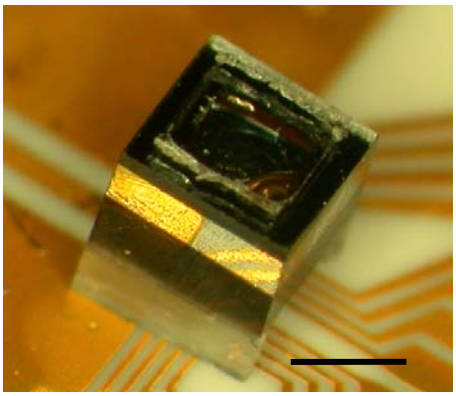

(b)

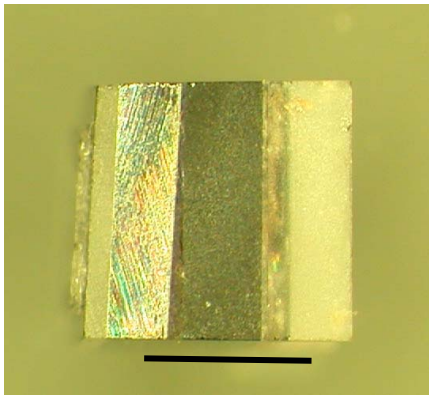

(c)

Figure 6 Optics sub assembly. (a) A schematic of the assembly showing the various layers using to condition the light. (b) a Photograph of the optics assembly mounted on the substrate. (c) A photograph of the optics assembly from the side. The black lines in the photographs indicate 1 mm.

The cell assembly was mounted to the top of the micro-optics package. The cell itself was fabricated from a 1-mm-thick piece of Si with a square hole 0.9 mm on a side etched in it. Glass wafers, 200 μm thick, sealed the cell from above and below. Also above and below the cell were two planar heater structures made from a film of Indium-

Tin oxide (ITO) deposited on a thin (125 μm) glass substrate. The ITO film was contacted with gold traces deposited on at the edges of the film to which gold wire bonds were attached. A schematic of the ITO heater construction and a photograph of the ITO heaters mounted to the cell are shown in Figure 7. When a current was passed through both ITO films, heat was generated, which raised the temperature of the cell to the point at which a strong optical absorption resonance was seen, roughly 80 ºC. The magnetic field produced by this current, which flowed in the same direction in the two heaters, did not noticeably affect the basic operation of the clock. A longitudinal magnetic field of 120 μT was applied to the structure with an external solenoid, and a large magnetic shield reduced stray fields near the cell.

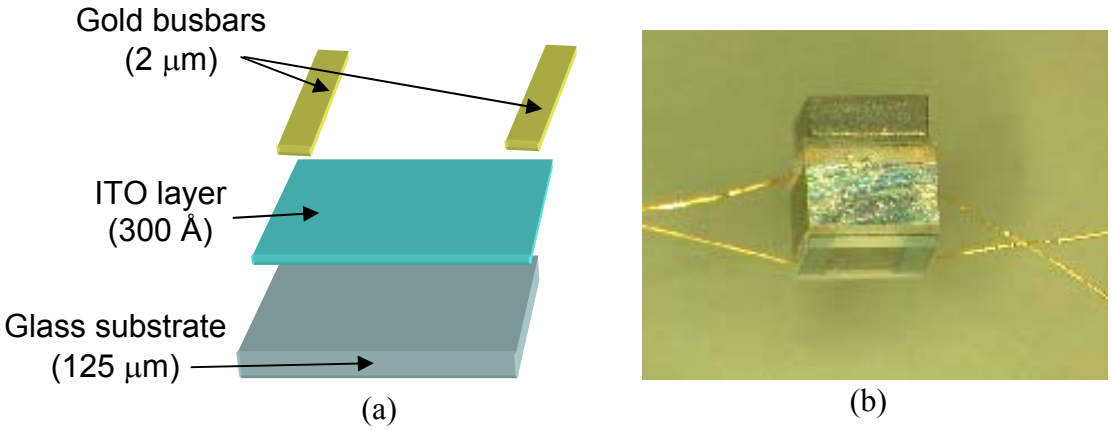

Figure 7 (a) Schematic of the ITO heater structures. (b) Photograph of ITO heater attached to the cell. Gold wires protrude from the sides of the ITO. The second ND filter noted in Figure 6a is attached to the lower heater unit.

Finally, a Si PIN photodiode mounted onto a glass substrate and surrounded by a Si spacer was mounted on top of the cell assembly to detect the light. The heaters and photodiode were electrically connected to the baseplate with gold wire-bonds.

Task 5: Assembly and Testing

The individual components were assembled using a high-temperature, transparent adhesive and the gold wire bonds that were attached to the heater and detector sub-assemblies before final integration were then bonded to the baseplate. The final assembly is shown in Figure 8. The operation of the frequency reference was based on coherent population trapping and therefore did not require the use of a microwave cavity around the atoms. Laser current modulation at 4.6 GHz was applied from a synthesizer, and the laser frequency stabilized such that the two first-order sidebands on the optical carrier were resonant with the optical transitions from the two components of the hyperfine-split atomic ground state to the $6P_{3/2}$ excited state. A CPT resonance was observed by sweeping the modulation frequency about the first subharmonic of the 9.2 GHz hyperfine transition; the detected resonance is shown in Figure 9. The resonance width of 7.1 kHz was dominated by power broadening from the optical field, although significant contributions were also present from diffusion of atoms to the cell walls and spin-exchange collisions. The contrast, which we define as the change in absorption due to the

CPT resonance divided by the Doppler absorption, was 0.91 % and was limited primarily by the large number of Zeeman sublevels in the ground state and by the presence of excited-state hyperfine levels not connected to both ground states. The small degradation in the contrast over that observed previously in other cells was probably due to the higher buffer-gas pressure used here, which broadened the optical transitions and therefore allowed for more single-photon excitation by the original optical carrier and higher-order FM sidebands.

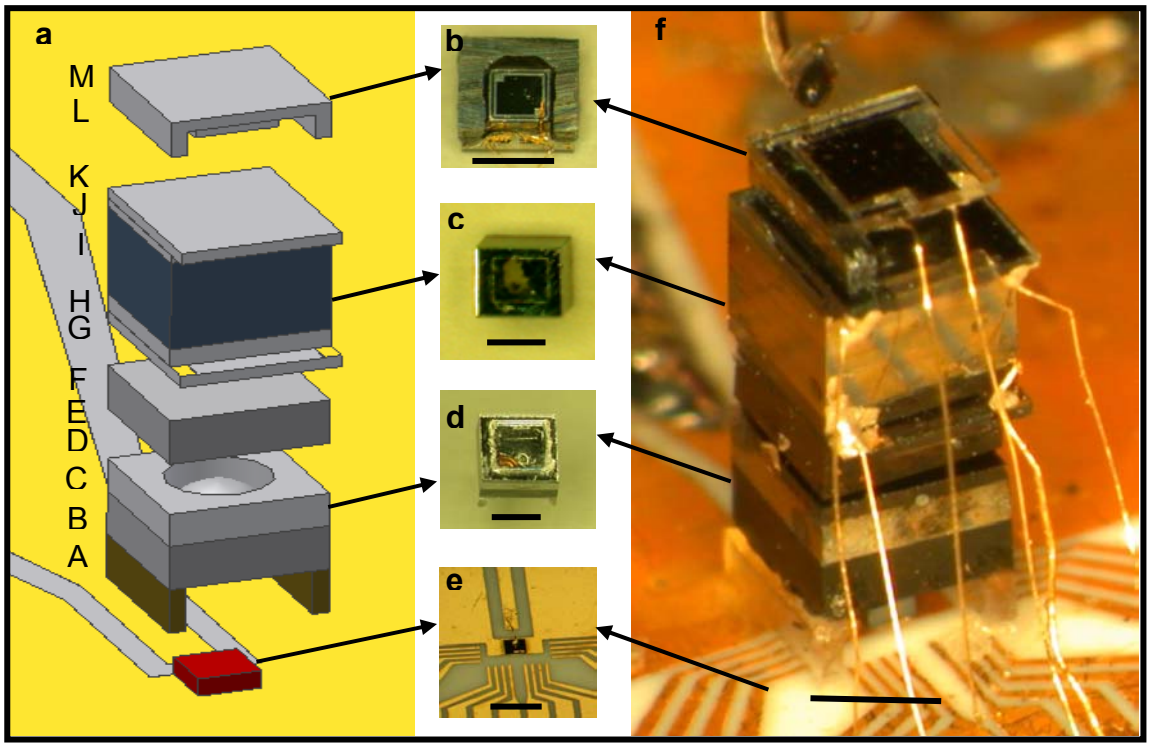

Figure 8 The microfabricated atomic clock physics package. a, Schematic of assembly. Layers from bottom to top: A, Glass (500 μm); B, ND filter (500 μm); C, Spacer (375 μm); D, Glass (125 μm, not shown); E, Quartz (70 μm, not shown); F, ND filter (500 μm); G, Glass/ITO (125 μm/30 nm); H, Glass (200 μm); I, Si (1000 μm); J, Glass (200 μm); K, Glass/ITO (125 μm/30 nm); L, Si (375 μm); M, Glass (125 μm). Total height, 4.2 mm, width and depth, 1.5 mm. Photographs b, photodiode assembly, c, cell assembly, d, optics assembly and e, laser assembly and f, the full atomic clock physics package realized as a microchip. The black lines in the photographs indicate 1 mm. The diode laser ran at a temperature of 46 ºC and with a DC injection current of 1.3 mA and a voltage of 2 V, producing 0.5 mW of optical power that was attenuated to 12 μW before the cell window by the ND filters. The ITO heater units heated the cell to about 80 ºC with a current of 53 mA and a voltage of 1.3 V. The magnitude of the magnetic field in the cell resulting from this current was expected to be below 10 μT. The RF power required to modulate the laser at 4.6 GHz was 70 μW.

The microwave frequency generated by the synthesizer was locked to the atomic transition by feeding the photodiode error signal back to the tuning port of the oven-controlled quartz crystal used as the reference for the synthesizer; the stabilized frequency was measured with respect to a more stable, secondary frequency source. The time-series data and Allan deviation are shown in Figure 10. As with most vapour-cell frequency references, the a priori determination of the absolute frequency is limited by the knowledge of the pressure of the buffer-gas that fills the cell. Under the assumption

that this pressure can be determined to within 1 %, the frequency reference as implemented here has a fractional frequency uncertainty of 5×10^{-8}. However, the long-term frequency stability and the frequency uniformity between many individual units are expected to be substantially better, particularly if the wafer-level fabrication methods discussed below are implemented.

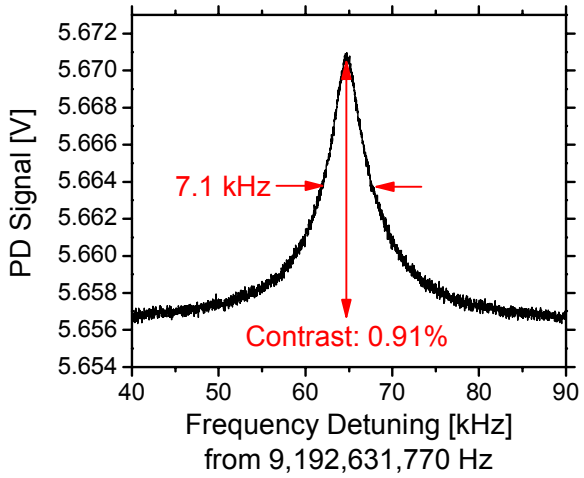

Figure 9 A CPT resonance measured in the CSAC physics package shown in Figure 8**.**

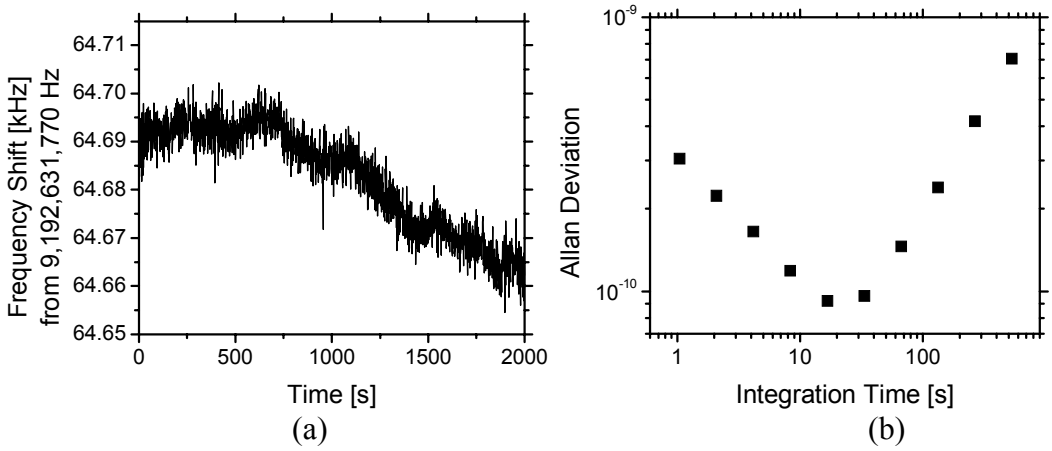

Figure 10 (a) The output frequency of the lock-up compact frequency reference as a function of time. (b) The corresponding Allan deviation.

The electrical power required to run the physics package, not including the base-plate heating, was 71 mW, and was dominated by the power required to heat the cell. A significant advantage obtained by using a VCSEL is the extremely low power required to both run the laser and to modulate it with sufficient amplitude to excite the CPT resonance. By modelling the heat flow in the structure, both analytically and with a finite-element computation, the heat loss channels could be roughly identified. We estimate that 30 mW is lost through the lower spacer unit, and that 24 mW is lost through the six gold wire bonds providing the electrical connections to the baseplate. The remainder is presumably lost through radiation and through conduction to the air surrounding the physics package.

Significant improvements in the thermal engineering are still possible and promise to reduce the power required to heat the cell to near 10 mW. The main heat loss sources are conduction from cell to baseplate through the lower spacer unit and the wire bonds, conduction to the air surrounding the package, and radiation. Conduction to the air surrounding the package could be reduced to a negligible level by packaging the physics package in a vacuum enclosure, as shown in Figure 11. If the gas pressure in the evacuated enclosure were significantly below ~ 1 Pa, the thermal conductivity should be negligible. Heat loss due to radiation between the cell and the shield is given by the Stefan-Boltzmann law:

$$\dot{Q} = \alpha\sigma\left(T_1^4 - T_0^4\right)A$$

where α is the emissivity, σ is the Stefan-Boltzmann constant A is the area of the radiating surface and T_1 and T_0 are the temperatures of the cell and surroundings respectively. If a gold coating, with emissivity 0.02, were placed on the interior of the shield, the heat loss due to radiation would be roughly 0.2 mW for a temperature difference of 50 C.

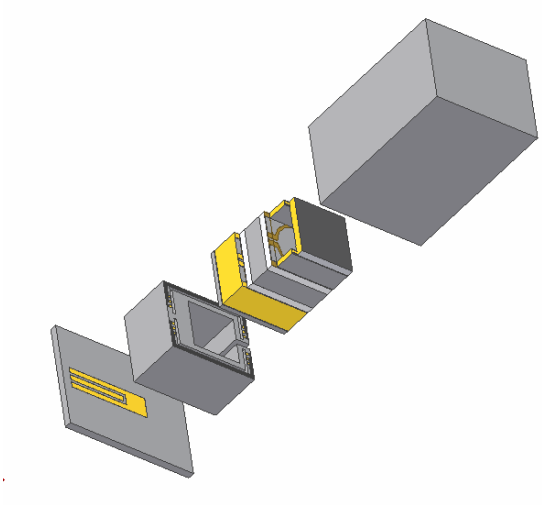

Figure 11 Advanced thermal isolation using a low-conductivity thermal isolation spacer and vacuum packaging of the cell sub-assembly.

Thermal conduction between the cell and the baseplate will be addressed with an advanced design for the thermal isolation spacer. The first modification to the existing spacer will be to use a material with a lower thermal conductivity. Pyrex has a thermal conductivity of 1.4 W/mK, while some polymer materials such as Teflon or SU-8 photoresist have thermal conductivities in the range of 0.2 W/mK, allowing a factor of 7 reduction in the power required to maintain a given temperature difference. For a spacer of height 1 mm and with walls of thickness 0.1 mm supporting the structure on its outside edges, the expected power dissipation is

$$\dot{Q} = I\left(T_1 - T_0\right)\frac{A}{L} \approx 7.2\ mW$$

for a temperature difference (T_1-T_0) of 50 ºC.

As single gold wire bond of diameter 25 μm and length 1 mm requires 8 mW to support at temperature difference of 50 ºC between its ends. Clearly some way of addressing the

heat flow through the electrical connections to the cell is needed. Our proposal is to use thin gold traces patterned on the top surface of the spacer to provide the thermal isolation. A diagram of how this might work is shown in Figure 12. Gold traces of width 10 μm, thickness 2 μm and length 1 mm would have a heat dissipation of 0.3 mW/trace for a ΔT of 50 K. Thus six traces would be expected to dissipate about 1.8 mW of power. The additional cross-sectional area of the spacer needed to support the traces would dissipate roughly an additional 2 mW. Thus the total expected power dissipation to support a ΔT of 50 K with both the advanced spacer unit and vacuum packaging is expected to be about 11 mW. Finite element analysis of the CSAC power dissipation yields similar results, as shown in Figure 13.

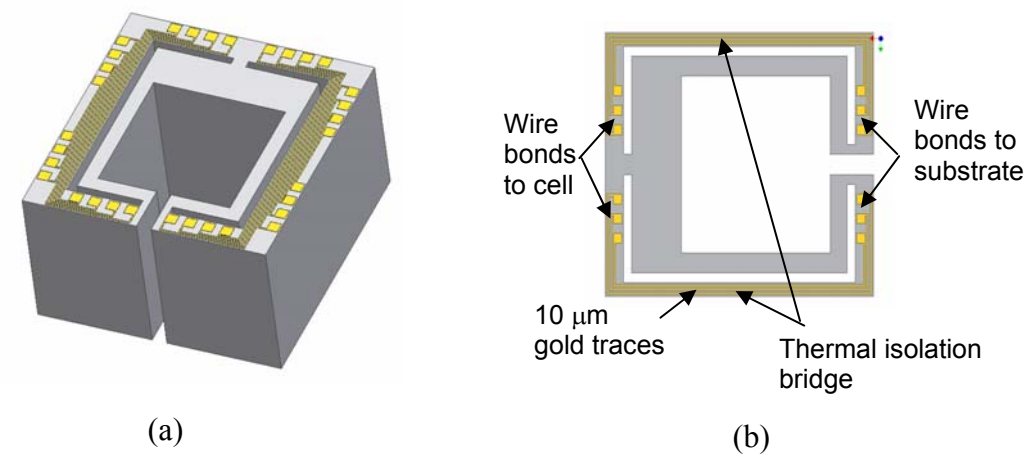

Figure 12 Thermal isolation of electrical connections from cell to baseplate. Thin gold traces, 10 mm wide are patterned on the top surface of the spacer. Wire bonds from the cell are connected to one end of the traces and wire bonds to the substrate are connected to the other end of the traces. The small cross-sectional area of the gold traces reduces the heat conduction.

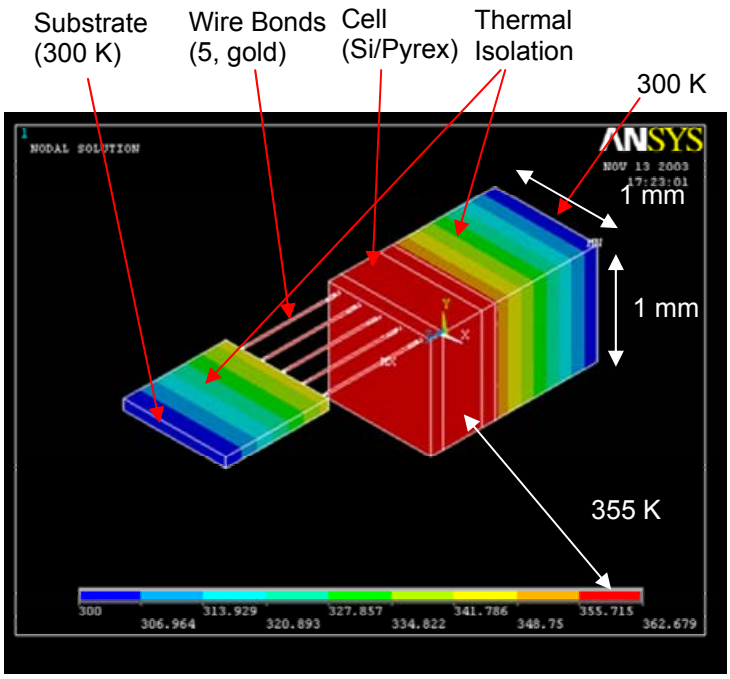

Figure 13 Finite-element thermal analysis of davnaced CSAC structure. Here a total of 5 mW of thermal power is input to the two faces of the cell. A temperature 55 K above ambient is achieved. Radiative losses are also included.

In addition to the power dissipated to heat the cell, the physics package has two other components that dissipate power. The laser DC power dissipation is about 2.6 mW at the current used here and the RF power required to modulate the laser at 4.6 GHz is 70 μW. The power required to provide a longitudinal magnetic field and sense the cell temperature should be well below 1 mW in the final design. With a total of 15 mW projected for the physics package, 15 mW remain for the local oscillator and control circuitry. The control circuit is being made by a small company and will be based on a small, low-power microprocessor. Running at 3 MHz, this processor should be able to implement all the CSAC control circuits with a power dissipation of 4.5 mW. This leaves 10 mW for the local oscillator, which should be sufficient, given the LO phase noise requirements outlined in the previous report (Sept. 03).

A summary of the final CSAC power budget is included below.

Component	Power	Confidence
Heating of cell (modeling):	11.1 mW	high
Diode laser DC power (measured):	2.6 mW	high
Diode laser RF power (measured):	70 mW	high
Local oscillator (estimate):	10 mW	low
Control circuit (MPU, 3 MHz, Ceyx):	4.5 mW	med.
B-field, temperature sensor, etc. (est.):	< 1 mW	high
Total:	**29.3 mW**	**med.**

Conclusion/Summary

We have constructed the first operating chip-scale physics package for an atomic clock. This physics packages is a vertically-integrated structure based on CPT excitation of the atomic D2 transition in a thermal Cs vapor. The structure comprises an optics sub-assembly, a cell sub-assembly and a photodetector sub-assembly which together are composed of 13 individual layers. The volume of the structure is 9.5 mm^3, having a square cross-section 1.5 mm wide and a height of 4.2 mm. The power required to run the cell at 80 ºC is 69 mW and the fractional frequency instability at one second is 3×10^{-10} as measured by the Allan deviation. The structure is amenable to wafer-level processing and assembly, enabling a large number of physics packages to be made with the same process sequence.

Thermal analysis indicates that the power required to heat the cell to 50 K above ambient could be less than 12 mW if advanced thermal engineering improvements are implemented. These include vacuum packaging of the assembly in a low-emissivity containment vessel, the addition of an advanced spacer unit with a lower thermal conductivity and the use of thin gold traces to provide the electrical connections to the package. With about 3 mW required to run and modulate the laser, 15 mW remain of the 30 mW DARPA program goal for the local oscillator and control electronics.

List of Publications/Presentations

Publications to date:

J. Kitching, S. Knappe and L. Hollberg, "Miniature vapor-cell atomic frequency references," Appl. Phys. Lett., **81**, 553, 2002.

M. Stahler, R. Wynands, S. Knappe, J. Kitching, L. Hollberg, A. V. Taichenachev and V. I. Yudin, "Coherent population trapping resonances in a thermal Rb^{85} vapor: D_1 versus D_2 excitation," Opt. Lett., **27**, 1472, 2002.

S. Knappe, V. Velichanski, H. G. Robinson, J. Kitching and L. Hollberg, "Compact vapor cells fabricated by laser-induced heating of hollow-core glass fibers," Rev. Sci. Instrum., **74**, 3142, 2003.

A. V. Taichenachev, A. M. Tumaikin, V. I. Yudin, M. Stahler, R. Wynands, J. Kitching and L. Hollberg, "Dependence of non-linear resonance lineshape on the transverse intensity distribution in a light beam," Accepted for publication, Phys. Rev. A.

A. V. Taichenachev, V. I. Yudin, R. Wynands, M. Stahler, J. Kitching and L. Hollberg, "Theory of dark resonances for alkali atoms in a buffer-gas cell," Phys. Rev. A **67**, 033810, 2003.

S. Knappe, J. Kitching and L. Hollberg, "Dark-Line Atomic Resonances in Sub-Millimeter Structures," accepted, Opt. Lett.

L. Liew, S. Knappe, J. Moreland, Hugh Robinson, Leo Hollberg and John Kitching, "Microfabricated Alkali Atom Vapor Cells," accepted Appl. Phys. Lett.

J. Kitching, S. Knappe, L. Liew, P. Schwindt, V. Shah, J. Moreland and L. Hollberg, "A Micromachined Atomic Clock," submitted to Nature.

Conference presentations to date:

J. Kitching, S. Knappe and L. Hollberg, "Performance of small-scale frequency references," International Frequency Control Symposium, New Orleans, LA, May 28-30, 2002.

J. Kitching, S. Knappe, L. Hollberg, "Ultra-small atomic frequency references," International Quantum Electronics Conference, Moscow, Russia, June 22-27, 2002.

S. Knappe, V. Velichansky, H.G. Robinson, J. Kitching, L. Hollberg, "Atomic vapor cells for miniature frequency references," Proc. IEEE Freq. Cont. Symp., Orlando, FL, May 29-31, 2003.

J. Kitching, S. Knappe, H. G. Robinson, L. Hollberg, L. Liew and J. Moreland, J. Maclennan, V. L. Velichansky, "Millimeter-Scale Atomic Frequency References,"

Presented at the annual conference of the Division of Atomic, Molecular and Optical Physics of the American Physical Society (DAMOP), Boulder, CO, May 20-24, 2003.

J. Kitching, S. Knappe, L. Liew, J. Moreland, S. Kargopoltsev, V. L. Velichanski, H. G. Robinson, L. Hollberg, "Ultra-Small Atomic Clocks based on Coherent Population Trapping and Micromachined Vapor Cells," presented at the 16th International Conference on Laser Spectroscopy, Palm Cove, Australia, July 13-18, 2003.

Li-Anne Liew, Svenja Knappe, John Moreland, Hugh Robinson, Leo Hollberg and John Kitching, "Micromachined Alkali Atom Vapor Cells for Chip-Scale Atomic Clocks," Presented at 17th International Conference on Micro Electro Mechanical Systems, Maastricht, Netherlands, Jan 25-29, 2004.

Patents to date:
J. Kitching and L. Hollberg, "Miniature frequency standard based on all-optical excitation and a micro-machined containment vessel," filed July, 2002 with USPTO, accepted Feb. 4, 2004.

J. Kitching, L. Hollberg, S. Knappe and R. Wynands, "A method of minimizing the short-term frequency instability of laser-pumped atomic clocks ," filed July, 2002 with USPTO.

J. Kitching, L. Hollberg, S. Knappe, L. Liew and J. Moreland, "Micromachined alkali-atom vapor cells and method of fabrication," in preparation.